PCCP

Accepted Manuscript

ROYAL SOCIETY OF CHEMISTRY

www.rsc.org/pccp

Journal Name

RSCPublishing

ARTICLE

Long-term self-assembly of inorganic layered materials influenced by the local states of the interlayer cations

Cite this: DOI: 10.1039/x0xx00000x

Received 00th January 2012,
Accepted 00th January 2012

DOI: 10.1039/x0xx00000x

www.rsc.org/

Kiminori Sato,[a] Kazuomi Numata,[a] Weili Dai[b] and Michael Hunger[c]

A wide variety of parameters as, e.g., temperature, humidity, particle size, and cation state are known to influence the agglomeration process of two-dimensional (2D) nanosheets, called self-assembly, in inorganic layered materials. The detailed studies on which parameters are decisive and how they influence the self-assembly, however, have not been performed yet. Here, the long-term self-assembly was studied for layered stevensite and hectorite, and compared with our previous data of saponite for elucidating an influence of local states of the interlayer cations. The results were analyzed with respect to a recently established rheological model, in which 2D nanosheets migrate parallel to the layer direction aided by water molecules as lubricants [K. Sato et al., *J. Phys. Chem. C* 2012, **116**, 22954]. With decreasing the strength of the local electric fields facing to the interlayer spaces, cation positions split into two or three, which makes the distribution of water molecules more uniformly. These water molecules enhance the rheological motion of the 2D nanosheets parallel to the layer direction, thus accelerating the self-assembly process.

Introduction

In inorganic layered materials, nanoscale two-dimensional (2D) sheets, denoted as 2D nanosheet, spontaneously agglomerate in a highly ordered manner via their mutual interactions with the aid of aqueous substances, such as, e.g., H_2O molecules.[1] This auto-agglomeration process enhanced by H_2O molecules, the so-called molecular self-assembly of 2D nanosheets, is increasingly of importance for dealing with global environmental issues.[2-4] For example, long-term self-assembly in layered saponite creates novel types of local structures, in which Cs cations are bound so strongly that they cannot be removed by strong hydrochloric acid solution.[2] In the recent model of giant earthquake nucleation, hydration of pore fluid in the interlayer spaces of clay minerals is associated with earthquake slip, which may lead to a weakening of plate-boundary faults.[3-4] Besides the global environmental issues, self-assembly is nowadays a disciplined technique for nanofabrication being not accessible for conventional techniques of materials synthesis.[5-7]

Smectites are inorganic layered materials with 2D nanosheets consisting of tetrahedral and octahedral units, which undergo a self-assembly aided by H_2O molecules existing in the Ångstrom-scale interlayer spaces. It is anticipated that the self-assembly is influenced by a wide variety of parameters as, e.g., temperature, particle size, humidity, cation state etc. X-ray diffraction (XRD) experiments at different temperatures and humidities provide the information on the basal spacing varied with cation species.[8-10] This implies that the local state of the interlayer cations is one of the most controlling factors for the process of self-assembly. Little is, however, known on the local states of the interlayer cations and their influence on the self-assembly process, because of the difficulty of probing the cation states inside the interlayer spaces.

In our former work,[12] the relationship between the interlayer cation states and the local structure of the 2D nanosheets was investigated by solid-state ^{23}Na nuclear magnetic resonance (NMR) spectroscopy for three kinds of smectites: saponite, stevensite, and hectorite, in which minor compositional fluctuations were introduced into the 2D nanosheets. Various well-defined cation states, susceptible to the local structure of the 2D nanosheets, were identified in the interlayer spaces. In saponite, charged tetrahedra inside the 2D nanosheets have a direct influence on the interlayer spaces. By this way, they cause a well-defined single cation state at the hexagonal cavities on the surface of the 2D nanosheets. In stevensite and hectorite, on the contrary, charged octahedra have an indirect influence on the interlayer spaces, splitting the dominant cation state into two and three, respectively. These materials with well-defined cation states are highly suitable for

investigating the influence of the interlayer cations on the long-term self-assembly process.

In parallel to that, we recently succeeded in establishing a rheological model for the long-term self-assembly of a Na^+-form saponite containing two kinds of local structures built by the insertion of one and two 2D nanosheets into the interlayer spaces.[13] In this model, the self-assembly involves two successive processes: adsorption of H_2O molecules due to hydration and water-assisted rheological motion of the 2D nanosheets. In result of hydration, H_2O molecules adsorb at Na cations in the interlayer space. H_2O molecules in the interlayer spaces immediately trigger off the rheological motion of the 2D nanosheets parallel to the layer direction. One of the two nanosheets inserted into the interlayer spaces are gradually released away. The local structure of one-nanosheet insertion thus gets to dominant for the self-assembled saponite.

In this study, the long-term self-assembly ranging from the onset of the H_2O adsorption at the interlayer cations to far after complete hydration is studied for saponite, stevensite, and hectorite with a single, two, and three cation states, respectively. The data of stevensite and hectorite obtained in the present study were analyzed on the basis of the above-mentioned rheological model together with our previous data of saponite, enabling comparative studies for an influence of interlayer cations. The aim of the present work is to answer the following questions: 1. Is the local cation state of significance for hydration? 2. Does the local cation state influence the self-assembly process? 3. What is the controlling factor for the initial hydration and successive self-assembly?

TABLE I. Chemical compositions in wt% and averaged particle diameters of saponite, hectorite, and stevensite.

	Saponite	Hectorite	Stevensite
SiO_2	54.71	56.41	56.70
Al_2O_3	5.02	0.04	0.05
Fe_2O_3	0.03	---	---
MgO	30.74	27.50	27.51
Li_2O	---	1.12	---
Na_2O	2.15	6.32	6.90
CaO	0.07	0.14	0.13
SO_3	0.67	1.10	1.18
H_2O	6.64	7.35	7.48
Diameter [nm]	92	45	37

Experimental section

Smectite materials

Synthetic Na^+-form saponite, hectorite, and stevensite developed by Kunimine Industries Co. Ltd. Japan were studied in the present work. They are aluminosilicates and commonly possess a 2 : 1 layered structure of 2D nanosheets consisting of tetrahedra and octahedra as shown in Fig. 1. The states of interlayer cation induced by the local structure of the 2D nanosheets in these smectites were studied by solid-state ^{23}Na NMR spectroscopy in our former work. [12] Basically, the O and Si atoms are located at the vertices and the central site of each tetrahedron, respectively. The vertices of the octahedra are occupied by O atoms and OH groups, whereas metallic elements, such as Mg and Li atoms, occupy the central sites. Table I lists the chemical compositions and particle diameters of saponite, stevensite, and hectorite, which are provided by Kunimine Industries Co. Ltd. As seen in the image of field emission scanning electron microscopy (FE-SEM) observed for saponite, an agglomeration of sheet-shaped particles up to a few μm occurs commonly for three kinds of smectimes (see Fig. 2). In the case of saponite, ca. 9.5 % of the central Si^{4+} atoms of the tetrahedra are replaced by Al^{3+} atoms, which leads to negatively charged tetrahedra (ca. 0.38 e^-) facing to the interlayer space. The electrostatic fields of the charged tetrahedra have a direct influence on the interlayer spaces, causing a well-defined single cation state for Na cations located at hexagonal cavities on the surface of the 2D nanosheets (see Na^+ position 1 in Fig. 1). In hectorite, on the contrary, ca. 10.3 % of the central Mg^{2+} sites of the octahedra are occupied by Li^+ atoms, while in stevensite, ca. 6.7 % of these sites are not occupied like a defect. These compositional fluctuations lead to negatively charged octahedra in hectorite (ca. 0.31 e^-) as well as stevensite (ca. 0.41 e^-).

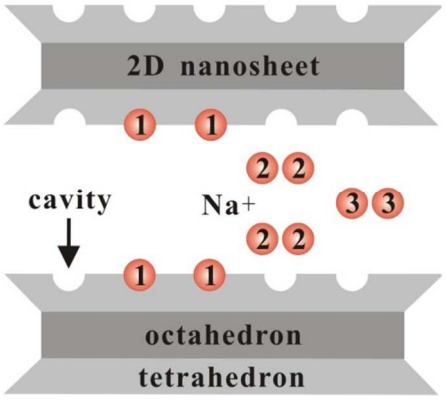

Fig. 1 Schematic illustration of layered structure of 2D nanosheets. The positions of Na cations inside the interlayer space are assigned with 1, 2, and 3.

In stevensite, the local electrostatic fields induced by the charged octahedra splits the dominant cation state at the hexagonal cavities into two. Hence, an additional cation state located slightly away from the surface of the 2D nanosheets is formed (see Na^+ position 2 in Fig. 1). In hectorite, the lower charges of the octahedra influence the interlayer space more moderately than those of stevensite. This causes a further splitting of the cation states into three, thus forming an additional cation state located far away from the surface of the 2D nanosheets (see Na^+ position 3 in Fig. 1).

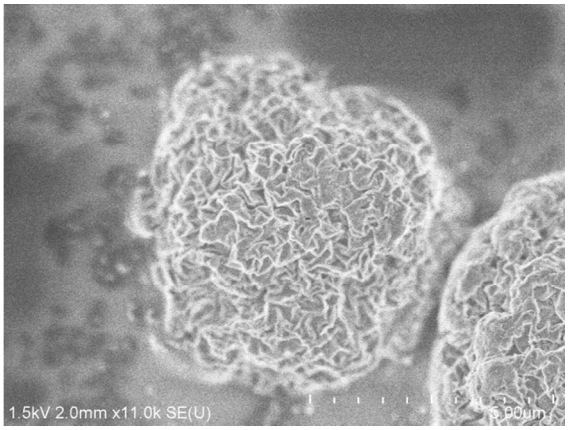

Fig. 2 FE-SEM image of saponite.

Gravimetric adsorption studies

Water adsorption was investigated via gravimetric measurements of the weight gain. The time-dependent gravimetric data were obtained using a TG-DTA system (TG-DTA 2020SA, BRUKER AXS Co. Ltd.) at room temperature with α-corundum (α-Al_2O_3) as an internal standard. The starting (dehydrated at 423 K for 12 h under a vacuum of ca. 10^{-5} Torr) samples were exposed to the humidity of 35 % at the temperature of 300 K, where the time-dependent data were obtained.

Solid-state ^{1}H nuclear magnetic resonance (NMR)

The ^{1}H MAS NMR studies of the water adsorption were performed on a Bruker Avance III 400WB spectrometer at the resonance frequency of 400.1 MHz, with 4 mm-Bruker rotors, the sample spinning rate of 10 kHz, a π/2 flip angle, and the repetition time of 10 s. The starting (dehydrated, vide supra) samples were exposed to the humidity of 35 % at the temperature of 300 K for 0 min, 15 min, 35 min, 1 h, 2 h, 5 h, and 10 h before recording the ^{1}H MAS NMR spectra.

Characterization of the open spaces

The sizes of the open spaces and their fractions were investigated by positronium (Ps) annihilation lifetime spectroscopy.[14-17] A fraction of the energetic positrons injected into the samples forms the bound state with an electron, which is called Ps. Singlet *para*-Ps (*p*-Ps), with the spins of the positron and electron antiparallel, and triplet *ortho*-Ps (*o*-Ps), with parallel spins, are formed at a ratio of 1 : 3. Hence, three states of positrons: *p*-Ps, *o*-Ps, and free positrons exist in the samples. The annihilation of *p*-Ps results in the emission of two γ-ray photons of 511 keV with the lifetime ca. 125 ps. Free positrons are trapped by negatively-charged elements, such as polar elements, and annihilated into two photons with the lifetime of ca. 450 ps. Positrons in the state *o*-Ps undergo a two-photon annihilation with one of the bound electrons with a lifetime of few nanoseconds after entering the Ångstrom-scale pores. The latter process is known as *o*-Ps pick off annihilation and provides information on the free volume R via its lifetime τ_3 according to the Tao-Eldrup model:[18-19]

$$\tau_3 = 0.5\left[1 - \frac{R}{R_0} + \frac{1}{2\pi}\sin\left(\frac{2\pi R}{R_0}\right)\right]^{-1} \quad (1)$$

where $R_0 = R + \Delta R$ and $\Delta R = 0.166$ nm is the thickness of homogeneous electron layer in which the positrons in the state *o*-Ps annihilate. The positron source (^{22}Na), sealed in a thin foil of Kapton, was mounted in a sample-source-sample sandwich. The starting (dehydrated, vide supra) samples were exposed to the humidity of 35 % at the temperature of 300 K, while Ps lifetime spectra were obtained every 45 min. The validity of the lifetime measurements and the data analysis was confirmed with certified reference materials (NMIJ CRM 5601-a and 5602-a) provided by National Metrology Institute of Japan, National Institute of Advanced Industrial Science and Technology (AIST).[20-21] The positron lifetime spectra were numerically analyzed using the POSITRONFIT code.[22]

Results and Discussion

Fig. 3 shows the ^{1}H MAS NMR spectra for saponite (a), hectorite (b), and stevensite (c), recorded after different hydration times, called exposure time here, ranging from 0 to 10 h. The spectra of the three smectites vary similarly with the exposure time. The ^{1}H MAS spectra of the starting (dehydrated) samples exhibit signals of hydroxyl (OH) groups at the chemical shift of 0.3 ± 0.1 ppm. The signals of adsorbed water molecules begin to appear at the chemical shift of 3.4 ± 0.1 ppm for the exposure time of 15 min. The lower chemical shift in comparison with that observed for bulk water in strongly hydrated porous materials, such as in fully hydrated zeolites (4.8 ppm),[23] is caused by physisorption of water molecules at the surface atoms of the smectite. The adsorption state of the water molecules is thus expected to be similar to surface water for initially hydrated smectite. The water signal is gradually enlarged, and a peak shift toward higher chemical shifts up to 4 ppm occurs with increasing exposure time. This demonstrates that the surface water is altered to bulk water with increasing hydration degree.

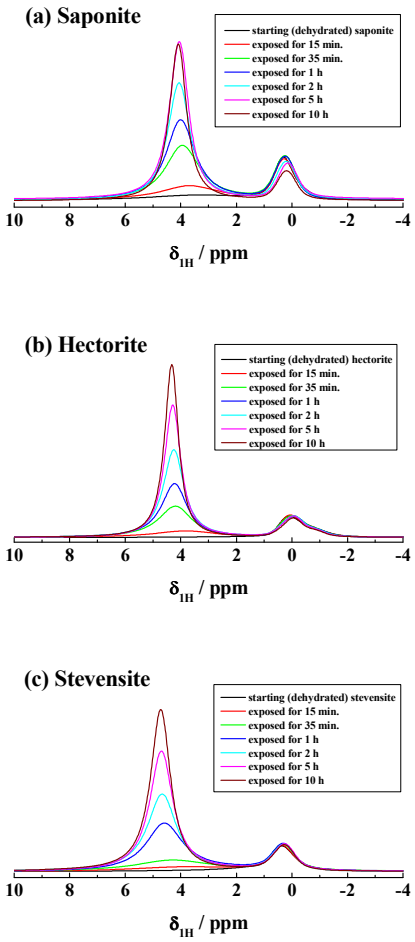

Fig. 3 ^{1}H MAS NMR spectra of saponite (a), hectorite (b), and stevensite (c) recorded after different exposure time ranging from 0 to 10 h. The data of saponite were taken from literature.[13]

By quantifying the water signals occurring at 3.4 to 4.0 ppm in the ^{1}H MAS NMR spectra of Fig. 3, the water concentration on the hydrated saponite, stevensite, and hectorite in Fig. 4 (a) were obtained. For comparison, the results of gravimetric measurements, also obtained as a function of the exposure time, are shown in Fig. 4 (b). The concentration of adsorbed H_2O molecules commonly increases for the three smectites with increasing exposure time up to ca. 8 h and remains constant above that. The data of saponite and stevensite at 10 h in Fig. 4 (a) are essentially the same as those of the fully hydrated materials, which indicates that adsorption of H_2O molecules at the Na cations in the interlayer spaces is completed. Similarly to the ^{1}H MAS NMR data, the gravimetric curves increase with the exposure time up to ca. 8 h owing to hydration of the interlayer spaces and are constant thereafter (see Fig. 4 (b)). By both methods, water adsorption capacities in the sequence of saponite > hectorite > stevensite were found.

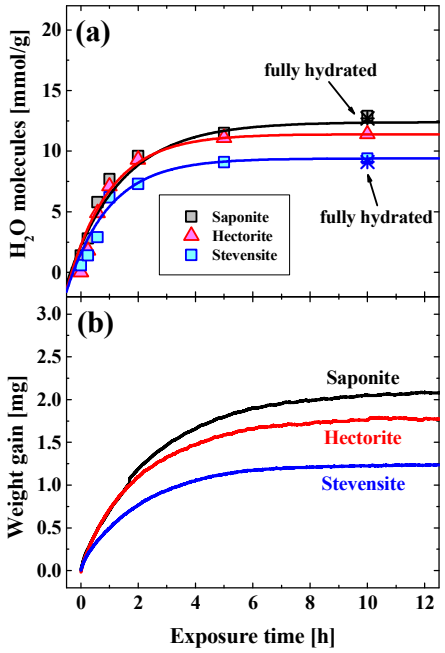

Fig. 4 Concentration of H_2O molecules adsorbed at saponite, hectorite, and stevensite, evaluated by comparing the ^{1}H MAS integral NMR intensities of the water signals with that of a standard zeolite (a), and gravimetrically obtained values, both plotted as a function of the exposure time (b). The solid lines in (a) are drawn for guiding the eye. The stars plotted at the exposure time of 10 h in (a) are the data of fully hydrated saponite and stevensite. The data of saponite were taken from literature.[13]

Considering the particle diameters of 92 nm for saponite, 45 nm for hectorite, and 37 nm for stevensite (see Table I), the volume fractions of the segmented interlayer spaces have the sequence of saponite > hectorite > stevensite. It is thus reasonably inferred that the volume of the segmented interlayer spaces is decisive for the water adsorption capacities of the smectites.

Ps annihilation spectroscopy reveals two kinds of open spaces denoted as A and B for the three kinds of smectites. In Fig. 5, the sizes of the open spaces R_A and R_B (top) and their fractions f_A and f_B (bottom) are presented as a function of the exposure time. These values show similar tendencies in their variation with the exposure time. The starting (dehydrated) samples commonly possess open spaces with sizes of $R_A \sim 0.3$ nm and $R_B \sim 0.9$ nm and corresponding fractions of $f_A \sim 5$ % and $f_B \sim 10$ %, respectively. The size R_A of the open space A is consistently ~ 0.3 nm without any significant change with increasing exposure time, whereas R_B decreases from ca. 0.9 to 0.6 nm. The fraction f_A gradually increases from ca. 5 to 15 % with the exposure time in contrast to the decrease of f_B from ca. 10 to 2 %. The time-dependences of R_B, f_A, and f_B are well-synchronized with exposure times up to 240 h. This is much longer than those of the hydration processes observed by solid-state NMR spectroscopy and the gravimetric measurements, going only up to 8 h.

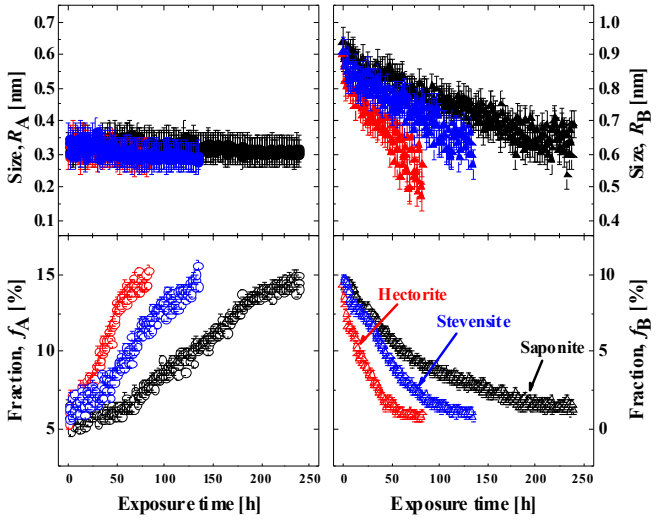

Fig. 5 Sizes R_A and R_B of open spaces A (solid circles in upper left) and B (solid triangles in upper right) with their fractions f_A (open circles in lower left) and f_B (open triangles in lower right), respectively, as a function of the exposure time for saponite (black symbols), hectorite (red symbols), and stevensite (blue symbols). The data of saponite were taken from literature.[13]

As is detailed in our former studies by means of *o*-Ps lifetime spectroscopy coupled with molecular dynamics (MD) simulation, the long-term variation of the open nanospaces observed for the present smectites is caused by a self-assembly with the modification of two kinds of local structures. This could not be probed by in-situ humidity-controlled XRD measurments. One of the local structures is called type II, in which one nanosheet is inserted into the interlayer space forming the open space with the size $R_A \sim 0.3$ nm. Another one is type I, in which two nanosheets are inserted into the interlayer spaces, forms the large open space with the size $R_B \sim 0.9$ nm. In the dehydrated state, the local structure of type I is the dominating one as deduced from the lower and higher fractions of f_A and f_B, respectively. H_2O molecules adsorbed at Na cations in the interlayer spaces due to hydration trigger off the rheological motion of the 2D nanosheets parallel to the layer direction. One of the two nanosheets inserted into the interlayer space of type I is thus released away, and the type II with the smaller open spaces A becomes the dominating one for the hydrated state. The released sheets could form the type II in the hydrated state. Hence, the open space size R_B decreases with increasing exposure time, while the open space size R_A remains constant. Correspondingly, the fraction f_A increases and the fraction f_B oppositely decreases with increasing exposure time. It should be noted here that the self-assembly probed by *o*-Ps lifetime spectroscopy is enhanced more efficiently in the sequence of hectorite > stevensite > saponite, in which the number of cation positions in the interlayer spaces increases from one to three as shown in Fig. 1. The sequence of the self-assembly is in contrast with that of water adsorption observed in the data of the solid-state NMR and gravimetric studies (see Fig. 3). This finding demonstrates that the above-mentioned rheological motion of the 2D nanosheets from the local structure of type I to that of type II is not influenced by the amount of H_2O molecules, but by the states of the Na cations.

Combining the data of the gravimetric studies, ^{1}H MAS NMR, and Ps annihilation spectroscopy together with our recent rheological model, we can describe, how the local structure as well as the volume of the interlayer spaces have an influence on the hydration-induced self-assembly process of smectites. H_2O molecules begin to adsorb at Na cations in the interlayer spaces and occupy adsorption states comparable with those of surface water. The surface water is altered to bulk water upon complete hydration within ca. 8 h. The H_2O adsorption capacity is dominated by the volume of the segmented interlayer spaces. H_2O molecules adsorbed at Na cations in the interlayer spaces trigger off the rheological motion of the 2D nanosheets parallel to the layer direction. One of two nanosheets inserted into the interlayer spaces are thus released away, which is aided by the adsorbed H_2O molecules. Local structures of type I are gradually altered to those of type II, which finally gets to dominant type for the self-assembled smectites.

The process of rheological self-assembly is sensitively influenced by the local structure of the 2D nanosheets. In saponite, a single cation position caused by the electrostatic fields of the charged tetrahedra is located at hexagonal cavities on the surface of the 2D nanosheets. These cations create a driving force of the H_2O adsorption, leading to more H_2O molecules located closely to the tetrahedral units of the 2D nanosheets. On the other hand, the two kinds of cation positions in stevensite make the distribution of H_2O molecules in the interlayer spaces more uniformly. Therefore, the 2D nanosheets can be smoothly released enabling the self-assembly more easily than in the case of saponite. The three kinds of cation positions in hectorite make this effect much stronger and the H_2O distribution more uniformly, further enhancing the self-assembly process.

Conclusions

The hydration-induced long-term self-assembly process was studied for inorganic layered stevensite and hectorite materials, and compared with our previous data of saponite. Gravimetric studies, ^{1}H MAS NMR spectroscopy, and Ps annihilation spectroscopy were combined with a recently established rheological model. H_2O molecules begin to adsorb at Na cations in the interlayer spaces and occupy adsorption states similar to those of surface water. Upon complete hydration of the smectites, the surface water is altered to bulk water. The water adsorption capacity was found to be determined by the volume of the segmented interlayer spaces. The hydration-induced H_2O adsorption at Na cations located in the interlayer spaces trigger off the rheological motion of the 2D nanosheets parallel to the layer direction. One of the two nanosheets

inserted into the interlayer spaces are thus released away, aided by H_2O molecules as lubricants. The local structures with the two-nanosheet insertion are gradually altered to those with the one-nanosheet insertion, and the latter finally dominates the self-assembled smectites.

The process of hydration-induced rheological self-assembly was found to be sensitively influenced by the cation positions, which are determined by the local structures of the 2D nanosheets. With decreasing the strength of the electrostatic fields in the interlayer spaces, cation positions split into two or three, making the rheological motion of the 2D nanosheets more smoothly due to an uniform H_2O distribution inside the interlayer spaces. Long-term self-assembly is thus accelerated with increasing the number of cation positions inside the interlayer spaces. This evidences that the local structures of the 2D nanosheets, determining the cation positions, are decisive for controlling the process of rheological self-assembly rather than the amount of H_2O molecules. The modification of the local structures of the 2D nanosheets could be thus a most straightforward strategy for the development of highly hygroscopic materials with large water adsorption capacities by employing the self-assembly. In addition, the clarification of the local structures of layered clay minerals as, e.g., contaminated materials at Fukushima, could reveal the mechanism of the heavily adsorption of Cs cations, which also depends on self-assembly. Therefore, the present findings are of particular importance not only for the design of new functional adsorbents, but also for a better understanding of global environmental issues, such as, e.g., giant earthquake nucleation and the above-mentioned specific Cs^+ adsorption.

Acknowledgements

The authors are indebted to K. Kawamura (Okayama University) and K. Fujimoto (Tokyo Gakugei University) for fruitful discussion. K. Sato would like to thank Alexander von Humboldt Foundation (AvH), Fachbereich Physik der Universitaet Stuttgart, and Max-Planck-Institute fuer Festkoerperforschung for their financial supports. M. Hunger thanks Deutsche Forschungsgemeinschaft for financial support. Finally, this work was partially supported by a Grant-in-Aid of the Japanese Ministry of Education, Science, Sports and Culture (Grant Nos. 25400318 and 25400319).

[a] Department of Environmental Sciences, Tokyo Gakugei University, Koganei, Tokyo 184-8501, Japan.
[b] Key Laboratory of Advanced Energy Materials Chemistry (Ministry of Education), College of Chemistry, Nankai University, Tianjin 300071, P. R. China.
[c] Institute of Chemical Technology, University of Stuttgart, 70550 Stuttgart, Germany.

References

1 G. M. Whitesides and B. Grzybowski, *Science*, 2002, **295**, 2418.
2 K. Sato, K. Fujimoto, W. Dai, and M. Hunger, *J. Phys. Chem. C*, 2013, **117**, 14075.
3 C. A. J. Wibberley and T. Shimamoto, *Nature*, 2005, **436**, 689.
4 K. Sato, K. Numata, and K. Fujimoto, *Inter. J. Nanoscience*, 2012, **11**, 12400331.
5 L. E. Walle, S. Agnoli, I. -H. Svenum, A. Borg, L. Artiglia, P. Krüger, A. Sandell, and G. Granozzi, *J. Chem. Phys.*, 2011, **135**, 054706.
6 L. Wu, J. Lal, K. A. Simson, E. A. Burton, and Y. Y. Luk, *J. Am. Chem. Soc.*, 2009, **131**, 7430.
7 Tae-Bong Hur, Tran X. Phuoc, and Minking K. Chyu, *J. Appl. Phys.*, 2010, **108**, 114312.
8 L. M. Toma, R. Y. N. Gengler, D. Cangussu, E. Pardo, F. Lloret, and P. Rudolf, *J. Phys. Chem. Lett.*, 2011, **2**, 2004.
9 M. S. Karmous, H. B. Rhaiem, J. L. Robert, B. Lanson, and A. B. H.. Amara, *Appl. Clay Sci.*, 2009, **46**, 43.
10 S. Morodome and K. Kawamura, *Clay Clay Miner.*, 2009, **57**, 150.
11 S. Morodome and K. Kawamura, *Clay Clay Miner.*, 2011, **59**, 165.
12 K. Sato, K. Numata, W. Dai, and M. Hunger, *Appl. Phys. Lett.* 2014, **104**, 1319011.
13 K. Sato, K. Fujimoto, K. Kawamura, W. Dai, and M. Hunger, *J. Phys. Chem. C*, 2012, **116**, 22954.
14 K. Sato, H. Murakami, K. Ito, K. Hirata, and Y. Kobayashi, *Macromolecules*, 2009, **42**, 4853.
15 K. Sato and W. Sprengel, *J. Chem. Phys.*, 2012, **137**, 1049061.
16 K. Sato, *J. Phys. Chem. B*, 2011, **115**, 14874.
17 Hamdy F. M. Mohamed, S. Kuroda, Y. Kobayashi, N. Oshima, R. Suzuki and A. Ohira, *Phys. Chem. Chem. Phys.*, 2013, **15**, 1518.
18 S. J. Tao, *J. Chem. Phys.*, 1972, **56**, 5499.
19 M. Eldrup, D. Lightbody, and J. N. Sherwood, *Chem. Phys.*, 1981, **63**, 51.
20 K. Ito, T. Oka, Y. Kobayashi, Y. Shirai, H. Saito, Y. Honda, Y. Nagai, M. Fujinami, A. Uedono, K. Sato, T. Hirade, A. Shimazu, H. Hosomi, and K. Sakaki, *J. Appl. Phys.*, 2008, **104**, 0261021.
21 K. Ito, T. Oka, Y. Kobayashi, Y. Shirai, K. Wada, M. Matsumoto, M. Fujinami, T. Hirade, Y. Honda, H. Hosomi, Y. Nagai, K. Inoue, K. Saito, K. Sakaki, K. Sato, A. Shimazu, and A. Uedono, *Materials Science Forum*, 2009, **607**, 248.
22 P. Kirkegaard and M. Eldrup, *Comput. Phys. Commun.*, 1974, **7**, 401.
23 M. Hunger, D. Freude, and H. Pfeifer, *J. Chem. Soc., Faraday Trans.,* 1991, **87**, 657.
24 D. Freude, in *Encyclopedia of Analytical Chemistry,* ed. R. A. Meyers, J. Wiley & Sons Ltd, Chichester, 2000, p. 12188.
25 H. Klein, H. Fuess, and M. Hunger, *J. Chem. Soc., Faraday Trans.,* 1995, **91**, 1813.